An RF Memristor Model and Memristive Single-Pole Double-Throw Switches

Nicolás Wainstein and Shahar Kvatinsky

Andrew & Erna Viterbi Faculty of Electrical Engineering

Technion - Israel Institute of Technology

Haifa, Israel 3200003

Email: nicolasw@campus.technion.ac.il, shahar@ee.technion.ac.il

Abstract—In this paper, we present a scalable physics-based model that accurately predicts the steady-state high-frequency behavior of memristive RF switches. This model is, to the best of our knowledge, the first lumped RF memristor model that includes device parasitics obtained from physical measurements reported in the literature. Furthermore, we propose two topologies (series and shunt) for non-volatile single-voltage-controlled Single-Pole Double-Throw switches using the proposed lumped RF memristor model. These topologies exhibit low insertion loss and high isolation. Adding non-volatility to RF switches will result in reduced power consumption.

I. INTRODUCTION

Memristive devices are two terminal passive circuit elements whose resistance is determined by the history of the applied voltage or current and retained whenever the voltage or current is no longer applied (*i.e.*, non-volatility) [1]. These devices can be used as switches with discrete states, as they exhibit nonlinear behavior with a High Resistive State (HRS) and a Low Resistive State (LRS).

The switching mechanism varies with the technology, though it is typically determined by the formation or rupture of conductive filaments between two electrodes owing to electrochemical reactions, ion migration and Joule heating [2]. Switching from HRS to LRS is called SET, while the opposite switching is called RESET. These devices have proven to be an attractive feature for several applications (*e.g.*, memory, logic and neuromorphic) due to their non-volatility, low switching time and energy, scalability, small footprint, and CMOS integration compatibility.

Recently, the use of memristive devices as RF switches has been proposed [3], [4], [5], exploiting their achievable low insertion loss (IL), high isolation (IS) and high cutoff frequency, which are desired characteristics in RF switches. The non-volatility of memristors implies that no bias voltage or current is required to maintain a particular state, hence reducing the energy consumption. Moreover, the small size of memristors could improve the density of transceiver chains in multiple-input multiple-output (MIMO) systems.

While several physical and mathematical models have been developed for memristors (*e.g.*, VTEAM [6]), the literature still lacks a precise and scalable lumped physical model that describes the behavior of the device at high frequencies, such as those in radio-frequency applications (RF). Such a model would be a fundamental asset for RF Memristive Switches (RFMS) with different structures and materials over a wide range of frequencies. This model could be used in RFIC design and simulation tools, and is necessary for the expansion of memristive technologies into RF applications.

In this paper, we present a scalable lumped model that predicts to a great extent RFMS physical behavior. The proposed model relies on the VTEAM model for the transient analysis (*i.e.*, describes the programming sweep) and introduces a structure-inspired lumped RLC circuit to describe its behavior at high frequency. We demonstrate the use of the lumped model by designing and evaluating two topologies of non-volatile Single-Pole Double-Throw (SPDT) RF switches with a single bias voltage. SPDT switches [7] play a vital role as control devices in several RF and microwave applications such as phase shifters, attenuators, and shared system resource access.

II. RF MEMRISTIVE SWITCHES

A. Previously Proposed RFMS

Previously proposed RFMS can be characterized as electrochemical metallization (ECM) memristors [2], consisting of a pair of electrochemically asymmetric metal electrodes separated by a small-scale gap or an insulator. At LRS, a thin metal filament shortens the electrodes, while at HRS the filament disappears. For instance, Fig. 1a shows the device structure presented in [3], where Ag and Ti/Au/Ag electrodes (active and inert, respectively) are separated by a 35 nm air gap. The device is fabricated over a SiO_2 surface in a high resistivity silicon substrate, in a Coplanar Waveguide (CPW) transmission line. The reported device presents an IL of ~0.3 dB and an IS of ~30 dB at 40 GHz, and a typical cut-off frequency of 35 THz. The LRS and HRS are achieved by applying, respectively, $3\ V$ and $-0.4\ V$ across the electrodes. The authors claim that frequencies above 40 GHz could be achieved by canceling undesired substrate moding effects that perturb the performance of the switch, for example by integrating the device in a grounded CPW structure.

Another RFMS, presented in [4] is a $10\ \mu m$ gapless-type ECM RFMS with Ag and Ni electrodes (active and inert, respectively). Measurements from 1 to 6 GHz demonstrate an IL of less than 0.5 dB and an IS better than 30 dB. The voltage/current required to change the state of the device is nominally $1\ V/10\ mA$ (SET) and $-1\ V/10\ mA$ (RESET). In [5], a $Cu/SiO_2/Al$ ECM RFMS is presented. This switch has been characterized at 0.15 GHz, achieving an IL of 1.6 dB and an IS of 20 dB. Regardless of its lower performance, when compared to the aforementioned RFMS, it stands out for its simple structure, and therefore its simpler fabrication process.
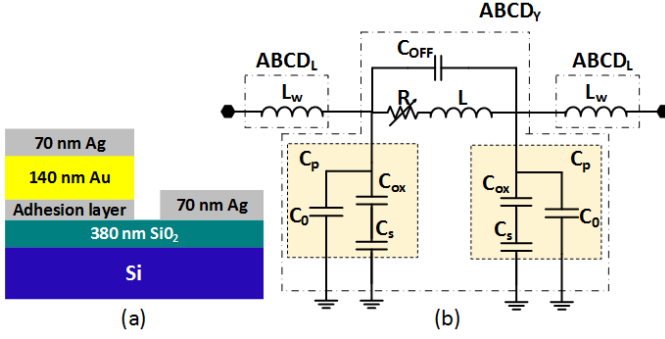
Fig. 1. (a) Memristive switch physical structure, as proposed in [3] (Reprinted by permission from Macmillan Publishers Ltd: Nat. Comm., copyright 2015), and (b) our proposed device model. The model is divided into three ABCD matrices (pointed rectangles), and $ABCD_Y$ is modeled as a Y-Parameter Π equivalent. The equivalent capacitors, C_p, are highlighted in yellow.

B. Previously Proposed Device Models

Models are indispensable tools in circuit design and simulation, as they simplify the understanding of the device and predict its behavior. Precise models for RFMS will allow accurate circuit designs and device optimization. In both [3] and [5], the RFMS is modeled as a simple parallel RC circuit. A first order analysis of the physical parameters is described in [3], where the LRS resistance and the gap capacitance (R_{ON} and C_{OFF}, respectively) are theoretically determined. Though the models are sufficiently accurate to describe the IL and IS of the device, they do not fully describe its S-parameters (i.e., their steady-state high-frequency electrical behavior). Furthermore, neither the skin effect of the conductors nor the fringe capacitance [8] at the electrodes are considered in these models. These effects will be dominant at high frequencies, and will determinate the RFMS performance and influence the matching network design.

An RF memristor model that predicts the maximum switching frequency in which a memristive memory cell can be operated is proposed in [9]. While this model considers further high-frequency phenomena, it is still a transient (time-dependent) model, thus not intended to describe the S-parameters of the memristor. In [10], a finite-difference time-domain implementation of the memristor using the non-linear ion drift model [11] is proposed. This model allows an electromagnetic-wave analysis of the memristor, yet it lacks the capacitive and inductive parasitics present in real devices.

III. PROPOSED RFMS LUMPED MODEL

A. Proposed Model Description

Based on an examination of the memristive device structure presented in [3], we propose a novel and more accurate model, shown in Fig. 1b. The model uses the two basic parameters from [3], R and C_{OFF}, where R represents the gap's resistance (i.e., describes the presence or absence of the filament) and C_{OFF} is the gap capacitance (i.e., capacitive coupling effect between the electrodes). Additional capacitors and inductors are added to represent the SiO$_2$ parasitic capacitance, C_{ox}, the Si substrate capacitance, C_s, and the fringe capacitance between the signal line and ground planes, C_0. The inductance of the filament and the electrodes are also considered and are, respectively, L and L_w. The inductors and capacitors are modeled as in [12].

The model is consistent with previous work in CPW and RF lumped device modeling [13]. Particularly, the device is considered as a gap discontinuity in the CPW at HRS and as a high impedance short-line section at LRS. The assumptions made in this model are (a) lossless substrate (i.e., high resistivity silicon), and (b) identical and perfect conductor electrodes (i.e., equal L_w and zero resistance in both electrodes).

B. Physical Parameters

The lumped elements in the proposed model can be determined directly from the dimensional parameters of the RFMS. The ON-state resistance of the filament (at LRS) accounts for the skin depth of a conductor with finite thickness and is

$$R_{ON} = \frac{\rho_{fil}l_{gap}}{w_{fil}\delta(1 - e^{-t_{fil}/\delta})}, \tag{1}$$

where ρ_{fil}, l_{gap}, w_{fil}, t_{fil} are, respectively, the filament's resistivity, length, width and height. The skin depth is δ, and w_{fil} depends on the compliance current. The between-electrodes (gap) capacitance is modeled as

$$C_{OFF} = \frac{\varepsilon_0\varepsilon_{eff}A_{BE}}{l_{gap}}k, \quad k \in [1.3, 1.6], \tag{2}$$

where ε_{eff} is the effective relative permittivity in the CPW, A_{BE} is the electrodes' lateral section and k is a dimensionless constant that accounts for the fringe capacitance, which is between 30% to 60% of the parallel plate capacitance [14]. The SiO$_2$ parasitic capacitor is determined by the SiO$_2$ height t_{ox}, the electrode's width w_E and the SiO$_2$ relative permittivity ε_{ox}, and is

$$C_{ox} = \frac{\varepsilon_0\varepsilon_{ox}}{t_{ox}}(w_E + 1.5\ t_{ox}). \tag{3}$$

The silicon substrate capacitance C_s and the fringe capacitance C_0 are

$$C_s = 2(\varepsilon_{Si} - 1)\varepsilon_0 F_{Si}\ , \quad C_0 = 4\varepsilon_0 F_0, \tag{4}$$

where ε_{Si} is the silicon relative permittivity, F_{Si} is the silicon geometry factor, and F_0 is the air geometry factor at the electrodes. The filament and electrode inducances are

$$L = \frac{\mu_0}{4F_{0_{fil}}}\ , \quad L_w = \frac{\mu_0}{4F_0}, \tag{5}$$

where $F_{0_{fil}}$ and F_0 are, respectively, the air geometry factor at the filament and the electrodes.

C. Fitting the Model to Experimental Data

To extract the lumped parameters from experimental data [3], we perform a fitting procedure. As shown in Fig. 1b, the proposed model can be described as three cascaded two-port network $ABCD$-transmission matrices. Neglecting L_w, the circuit can be analyzed as a Y-equivalent Π two-port network, where

$$Y_{12} = -\left(\frac{1}{R + j\omega L} + j\omega C_{OFF}\right), \tag{6}$$

$$Y_{11} + Y_{12} = Y_{22} + Y_{12} = j\omega C_p, \tag{7}$$

where C_p is the equivalent capacitor as shown in Fig. 1b. The Y-equivalent Π is transformed to $ABCD$-parameters to define $ABCD_Y$. The total $ABCD$ matrix is the product of the three matrices and is then transformed to S-parameters.

Initial fitting is done using the Simulated Annealing [15] algorithm to search for the minimum RMS error between the experimental and modeled S-parameters. Seed values for

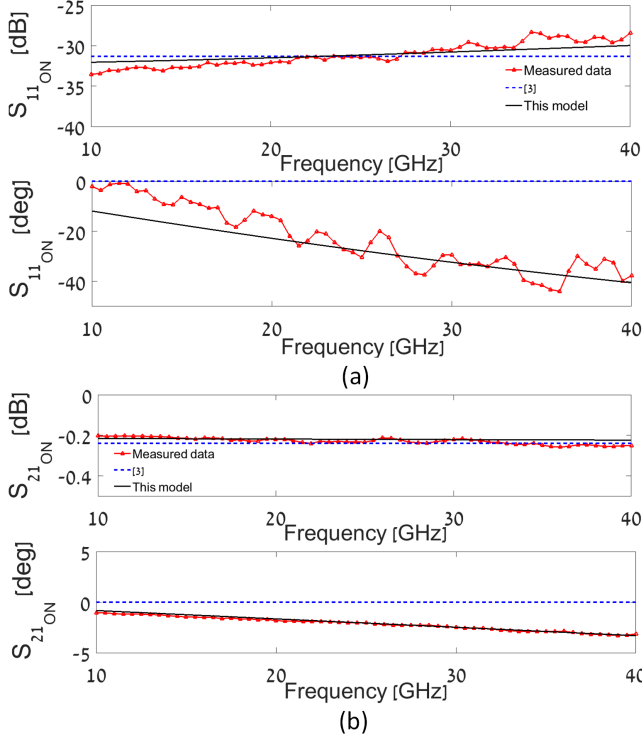| Parameter	Extracted parameters		Physical parameters
	[3]	This work	This work
R_{ON}	2.8 Ω	2.6 Ω	2.56 Ω
C_{OFF}	1.145 fF	1.145 fF	1.168 fF
C_p	-	3.08 fF	1.15 fF
L	-	77 fH	52 fH
L_w	-	3.7 pH	3.1 pH

Fig. 2. S-parameter simulation results as determined by the proposed model (black) and the RC model in [3] (blue dashed line) vs. experimental data (red line). (a) $S_{11_{ON}}$ and (b) $S_{21_{ON}}$.

R and C_{OFF} can be determined as explained in the supplementary material of [3]. To achieve even more accurate results, the obtained value of L_w can be used to determine the $ABCD_Y$ and then transformed it to a Y matrix. Parameters C_p, L and R can be extracted by fitting (6) and (7). C_{OFF} is determined from the OFF-state (HRS) S-parameters, where $Y_{12} \simeq -j\omega C_{OFF}$. The extracted parameters from the fitting procedure are listed in Table I.

IV. RESULTS

The proposed model is evaluated in two different ways. First by comparing the proposed model against the model presented in [3] and then by examing the extracted parameters from the fitting procedure with respect to the physical parameters determined by (1)-(5). The first evaluation demonstrates the improvement in the device model as compared to [3]. The second provides an estimation of the proximity between the physics-based calculated parameters and the extracted parameters.

A. Comparison Between Models

Fig. 2 shows the results of our model and the RC model presented in [3] versus experimental results. To perform a fair comparison, the model in [3] is fitted to this experimental data. Although the RC model exhibits a good match with S_{21} magnitude, it can be observed that our proposed model improves the S-parameters' accuracy, particularly of the phase, which is crucial for phase-sensitive applications and for designing matching networks. This trend becomes even more significant when extrapolating to higher frequencies, where the devices become more capacitive, due to the increasing influence of the electrodes' impedance.

Table I lists the fitting parameters for both models. The overall improvement with respect to [3] in the phase RMS error is 87% and 33% for, respectively, the ON and OFF state. The OFF-phase RMS error is still significant and it is caused by S_{11} phase, which is lower than $90°$. The overall enhancement of the magnitude RMS error is 25% for the ON state when compared to [3]. The RC model is sufficiently accurate for the OFF-state magnitude so no significant improvement is observed.

B. Extracted Parameters vs. Physical Parameters

Table I shows that the extracted parameters and the physics-based parameters determined by (1)-(5) are almost identical. This confirms that the physical parameters accurately predict the high-frequency behavior of the RFMS. Additional improvements in the model should add an analytical expression of the fringe capacitance at the gap and add to C_p the equivalent capacitance of a step change [16]. To validate this model, further tests should be performed with different data sets and different devices, varying the electrode's size, the gap's size and the CPW structure.

V. RFMS SPDT TOPOLOGIES

RFMS exhibits high-performance characteristics, small size and non-volatility, which makes it an excellent candidate to become a building block in high-performance, low power SPDT switches. These switches fulfill important functions in many RF applications, such as controlling the RF signal flow and providing multiple access to shared resources. With the proposed model, more accurate simulations can be achieved, making it possible to test and design RF SPDT and other RF applications.

In this section, we present two different RFMS SPDT topologies, which make use of a single control-voltage (i.e., a single bias signal) to simultaneously toggle between LRS and HRS the two branches. The switch design is focused on achieving broadband matching (low return loss), high IS and low IL, while utilizing only a single memristor per output port and only one overall control voltage. The topologies have been simulated in Advanced Design System (ADS) from Keysight using the aforementioned model and CPW sections as in [3]. We assume that no self-switching occurs at the band of interest and we also assume cold-switching (i.e., switching occurs when the RF signal is applied).

A. Series Switch

Fig. 3a shows the proposed series topology, where one memristor per port is used (M1 and M2). The circuit works as follows: when $V_{ctrl} = 3V$, M2 switches to LRS and M1 to HRS, hence providing a conductive path for the RF signal from port P1 to port P3, while port P2 is isolated (observe the opposite connection). Reciprocal analysis is done when $V_{ctrl} = -3V$. Note that because the RESET mechanism is faster than the SET, particular care must be taken when designing the controller to provide a defined compliance current to protect the RFMS. The inductors act as RF chokes and
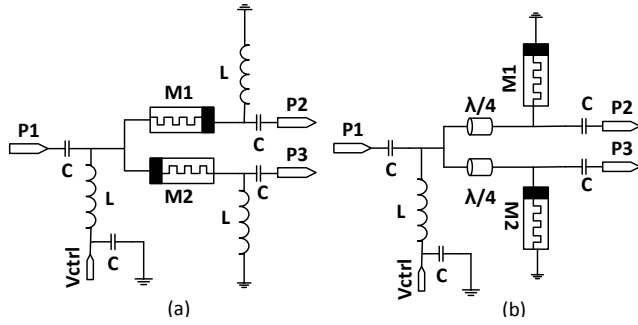
Fig. 3. Schematics of the proposed (a) Series and (b) Shunt RFMS SPDT topologies.
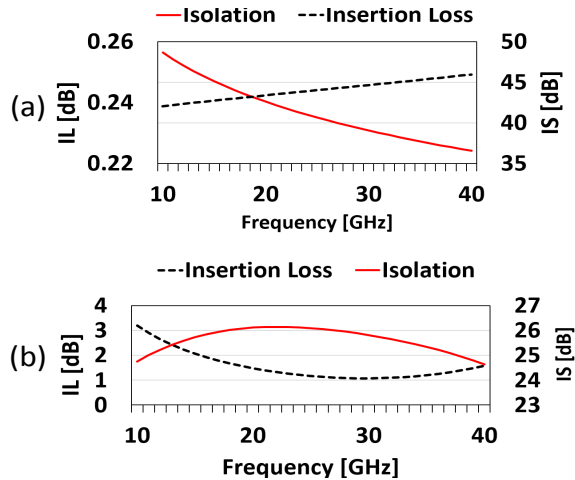

Fig. 4. Simulation results of IS (red) and IL (black dashed) of the proposed (a) Series and (b) Shunt SPDT topologies.

provide a DC reference for the memristors, while the capacitors provide RF feeding and DC blocking, thus avoiding floating nodes. Capacitors and inductors are considered ideal, as they could be part of a bias tee. Fig. 4a shows simulation results, where the IS is over 36 dB and the IL is below 0.26 dB at the designed band. It presents a broadband performance over the desired spectrum and the expected 6 dB improvement in IS as compared to [3].

B. Shunt Switch

Fig. 3b shows the shunt topology, where M1 and M2 have one terminal grounded. As in the series topology, when $V_{ctrl} = 3V$, M2 is in LRS and M1 is in HRS, and vice versa. The memristors provide a low resistive path to ground on LRS. This configuration makes use of the quarter-wavelength ($\lambda/4$) transmission line (designed for 30 GHz) to transform the short-circuit (whenever the memristor is at LRS) into a high-impedance path, thus isolating the desired branch. When the memristor is at HRS there is a direct RF path between ports in the branch. However, owing to the $\lambda/4$, the device becomes narrow-band and provides a lower IS than the series counterpart.

Simulation results for the shunt topology are shown in Fig. 4b. The narrow-band characteristic provides an IL of 1 dB and an IS of 26 dB at 30 GHz. Its performance is remarkably lower than the series SPDT since the losses derived from the $\lambda/4$. C_{OFF} and C_p provide a low impedance path to ground that diminish considerably its IS at higher frequencies. The

IS can be improved by resonating these capacitance with an inductance. However, as the RF path does not pass through the memristor, a higher power handling would also be expected.

VI. CONCLUSIONS

In this paper, we present a lumped RF memristive switch model that describes and accounts for different physical phenomena in the device structure. The model exhibits better accuracy than previously proposed models and is intended to promote the use of memristors in RF systems. We demonstrate the use of the proposed lumped model in two non-volatile single-voltage-controlled SPDT topologies. Both topologies show promising results, making them strong candidates for use in communication systems. Future work should focus on model validation with different data sets and devices and on the design of additional topologies for RF systems.

REFERENCES

[1] L. O. Chua, "Memristor–The Missing Circuit Element," *IEEE Trans. Circuit Theory*, vol. CT-18, no. 5, pp. 507–519, September 1971.

[2] R. Waser and M. Aono, "Nanoionics-based Resistive Switching Memories." *Nat. Mater.*, vol. 6, no. 11, pp. 833–40, November 2007.

[3] S. Pi, M. Ghadiri-Sadrabadi, J. C. Bardin, and Q. Xia, "Nanoscale Memristive Radiofrequency Switches." *Nat. Commun.*, vol. 6, no. 7519, pp. 1–9, June 2015.

[4] J. A. Nessel *et al.*, "A Novel Nanoionics-based Switch for Microwave Applications," *Proc. Int. Microwave Symp. Dig.*, pp. 1050–1054, June 2008.

[5] A. Vena *et al.*, "A Fully Passive RF Switch based on Nanometric Conductive Bridge," *Proc. Int. Microwave Symp. Dig.*, pp. 1–3, June 2012.

[6] S. Kvatinsky, M. Ramadan, E. G. Friedman, and A. Kolodny, "VTEAM: A General Model for Voltage Controlled Memristors," *IEEE Trans. Circuits Syst. II, Exp. Briefs*, vol. 62, no. 8, pp. 786–790, August 2015.

[7] R. Sorrentino and G. Bianchi, *Microwave and RF Engineering*. John Wiley & Sons, 2010.

[8] Y. Eo and W. R. Eisenstadt, "High-Speed VLSI Interconnect Modeling Based on S-Parameter Measurements," *IEEE Trans. Compon., Hybrids, Manuf. Technol*, vol. 16, no. 5, pp. 555–562, August 1993.

[9] A. Mazady and M. Anwar, "Memristor: Part II-DC, transient, and RF analysis," *IEEE Trans. Electron Devices*, vol. 61, no. 4, pp. 1062–1070, April 2014.

[10] M. D. Gregory and D. H. Werner, "Application of the Memristor in Reconfigurable Electromagnetic Devices," *IEEE Antennas Propag. Mag.*, vol. 57, no. 1, pp. 239–248, February 2015.

[11] E. Lehtonen and M. Laiho, "CNN using Memristors for Neighborhood Connections," *Proc. Int. Work. Cell. Nano. Netw. Appl.*, pp. 1–4, February 2010.

[12] W. Shu, H. Shichijo, and R. Henderson, "A Unified Equivalent-Circuit Model for Coplanar Waveguides With Silicon-Substrate Skin-Effect Modeling," *IEEE Trans. Microw. Theory Techn.*, vol. 64, no. 6, pp. 1–9, May 2016.

[13] W. Shu, S. Shichijo, R. Henderson, and X. An, "A Novel Model for Spiral Inductor based on a Unified CPW Circuit Model," *Proc. Annu. Wireless and Microwave Technology Conf.*, pp. 1–3, July 2014.

[14] G. M. Rebeiz, *RF MEMS: Theory, Design, and Technology*. John Wiley & Sons, 2003.

[15] S. P. Brooks and B. J. T. Morgan, "Optimization using simulated annealing," *J. R. Stat. Soc. Series D*, vol. 44, no. 2, pp. 241–257, 1995.

[16] R. N. Simons, *Coplanar Waveguide Circuits, Components, and Systems*. John Wiley & Sons, 2001.